Advanced InSAR interferometry for reservoir monitoring

Fabio Rocca,[1] and Alessio Rucci,[2] Alessandro Ferretti[2] and Adrian Bohane[3*] show, with a case study from the InSalah project, Algeria, the benefits of a new application of surface deformation monitoring using multi-interferogram permanent scatterer techniques, an advance form of radar interferometry.

Surface deformation monitoring provides unique data for observing and measuring the performance of hydrocarbon reservoirs, for enhanced oil recovery (EOR) and for carbon dioxide capture and sequestration (CCS). To this aim, radar interferometry (InSAR) and, in particular, have already proven to be valuable and cost-effective tools. For oil/gas reservoir management, PS measurements make it feasible to examine the temporal and spatial pattern of long-term reservoir response to pumping and extraction, highlighting possible compaction affecting the area surrounding the reservoir and generating potential damage to local infrastructure.

Apart from the environmental impact of subsidence and uplift phenomena induced by reservoir exploitation, recent optimization techniques ask for timely information about many geophysical parameters, both downhole and on the surface. In fact, depending on reservoir characteristics and depth, water, oil, or gas production/extraction can induce surface subsidence or, in the case of CCS, ground heave, potentially triggering fault reactivation and in some cases threatening well integrity.

Mapping the surface effects of pressure variations at the reservoir layer, due to either fluid extraction or injection, usually requires the availability of hundreds of measurement points per km^2 with millimetre-level precision, which is time-consuming and expensive to obtain using traditional monitoring techniques, but can be readily obtained with InSAR data.

Moreover, more advanced InSAR techniques (PSInSAR) developed in the last decade are capable of providing millimetre precision, comparable to optical levelling, and a high spatial density of displacement measurements, over long periods of time without need for installing equipment or otherwise accessing the study area. In this work we present examples of applications for reservoir monitoring and modelling with the aim of highlighting the importance of providing more and more accurate displacement measurements and the necessity to increase the density of measurement points in order to better constrain the reservoir parameters inversion.

Principles of SAR

In this section we briefly describe the SAR acquisition system and SAR Interferometry basic principles (Ferretti et al., 2007; Curlander and McDonough, 1992). A synthetic aperture radar (SAR) acquisition system consists of a moving antenna, assembled on a satellite (usually), that sends a signal towards a target and records the back-scattered signal, or in other words, its echo. The antenna beam looks laterally with respect to the flight direction. The signal pulses are sent, and recorded, at a frequency called pulse repetition frequency (PRF), which characterizes the sampling rate in the flight direction, called azimuth. The signal is modulated at radio frequency on transmission and demodulated on receiver, in phase and quadrature, so that it can be interpreted as a pair of real channels or a single complex channel. The received echoes are recorded into a regular grid, according on the azimuth location of the satellite and on the distance between the targets themselves and the sensor; the range distance (Figure 1).

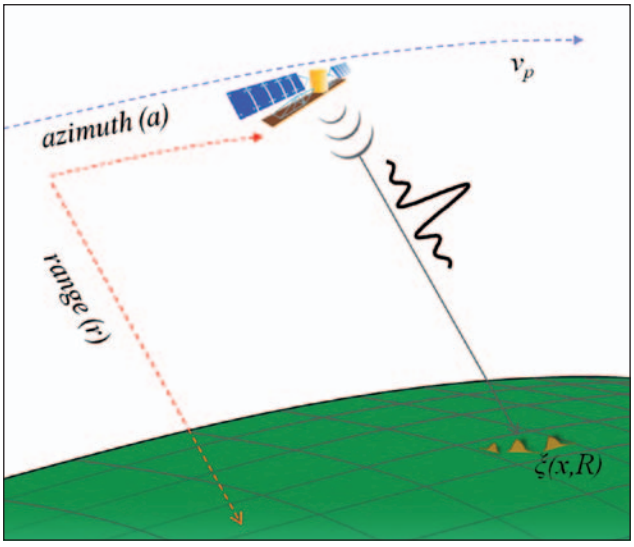

Figure 1 *Imaging geometry of SAR acquisition.*

[1] *Politecnico di Milano.*
[2] *TRE – Telerilevamento Europa.*
[3] *TRE Canada.*
[*] *Corresponding author, E-mail: adrian.bohane@trecanada.com*

© 2013 EAGE www.firstbreak.org

Then, as with seismic data processing, radar data has to be focused, as the same target at surface appears shifted in different azimuth bins. This coherent mechanism is often referred to as aperture synthesis and is the core principle SAR is built around. This mechanism is nothing else but seismic migration, as noticed in the past (Monti Guarnieri et al., 1990). The only differences with seismics are:

- Wavelength (now centimetres)
- Nature of the wave (electromagnetic rather than elastic)
- Very high uniformity of the velocity field, impaired only by the atmospheric water vapour, at is will be seen in the sequel
- Penetration in the terrain, of the order of the wavelength

According to this interpretation of focusing, the final image has a resolution which is close to the one we would have with a giant antenna, corresponding to the total distance covered by the platform while the target was in sight.

The resolution gain can be 1000, according to the sensor specifications. After the focusing compression the end-to-end SAR impulse response can be well approximated by a two-dimensional sinc (Ferretti et al., 2007):

$$h(r;\ a;\ R;\ x) \propto \xi(R;\ x)\,sinc\left[\frac{2B_{RF}(r-R)}{c}\right] sinc\left[\frac{B_{az}(a-x)}{v_p}\right] exp(-j4\pi R/\lambda) \quad (1)$$

Where:

- B_{RF} is the radio-frequency bandwith of the sinc signal sent by the platform
- B_{az} is the processed azimuth bandwith
- r, a are the spatial coordinates respectively in range and azimuth
- c is the speed of the light
- v_p is the satellite velocity
- R is the target distance from the satellite
- λ is adopted wavelength
- $\xi\,(R; \chi)$ is the target reflectivity

The coherent nature of SAR data allows interferometric processing, if we look at equation 1 we notice a dependence on the distance between the target and the sensor. Such information can be used to measure the distance variations between successive acquisitions (Figure 1).

The key element for SAR interferometry is the interferogram which is the phase difference between two SAR images. Usually it is generated by taking the phase term of the hermitian product of two images, pixel by pixel, in such a way the reflectivity component of the phase, ξ, is cancelled out in the phase difference between two SAR images, and the remaining term is only due to propagation difference.

For sake of simplicity, the phase terms due to thermal noise, image misregistration, wrong focusing parameters, etc., will be neglected. Thus, the interferometric phase, $\phi_k\,(r, a)$, where k refers the image index, can be decomposed into different terms (Ferretti et al., 2007):

$$\phi_k(r,a) = \phi_{disp,k}(r,a) + \phi_{topo,k}(r,a) + \phi_{APS,k}(r,a) + \phi_{decorr,k}(r,a) \quad (2)$$

Analyzing in detail all the different terms. Let's start first with the phase variation due to topography, if a precise a priori digital elevation model (DEM) is available, we can compensate for this phase component before any analysis, otherwise we have to estimate the elevation error with respect to the available reference model. The phase term we are mainly interested in is the one related to surface motion, recalling equation 2, $\phi_{disp,k}(r, a)$ can be expressed analytically as follows:

$$\phi_{disp,k}(r,a) = -4\pi\Delta r/\lambda \quad (3)$$

where Δr is the component of displacement along the line of sight (LOS) which can be measured by the satellite (see Figure 2).

The term in equation 2, labeled $\phi_{APS,k}\,(r, a)$, is a noise source for our purposes, related to space-time variations in the vapour content in the atmosphere, which introduce a delay in the optical ray path, as observed before. The last term is still a noise term, related instead to decorrelation phenomena affecting the radar signature stability of the observed target. The radar response, in fact, can vary over time when temporal decorrelation occurs, and according to the geometry of each satellite acquisition, in case of geometrical decorrelation.

This last is due to the fact that, for the change in perspective dependent on the satellite position, the same spatial wavenumber (along the range direction) is illuminated by different radio frequencies, the higher, the lower is the elevation of the satellite on the horizon. Too high a change in elevation would remove any correlation altogether, owing to the limited radio frequency band used by the radar. Just for an order of magnitude, the relative change in frequency is approximately equal to the change of elevation in radians (Ferretti et al., 2007) i.e., 1^0 elevation change corresponds, for a centre frequency of 10 GHZ, to a 50 MHz shift of the frequency corresponding to the same ground wavenumber.

These two noise terms represent the main issues for SAR interferometry towards the millimetre accuracy in the measurement of surface displacement. In fact the accuracy achievable with traditional differential SAR interferometry (DInSAR), due to these noise sources, is in the order of centimetres.

www.firstbreak.org © 2013 EAGE

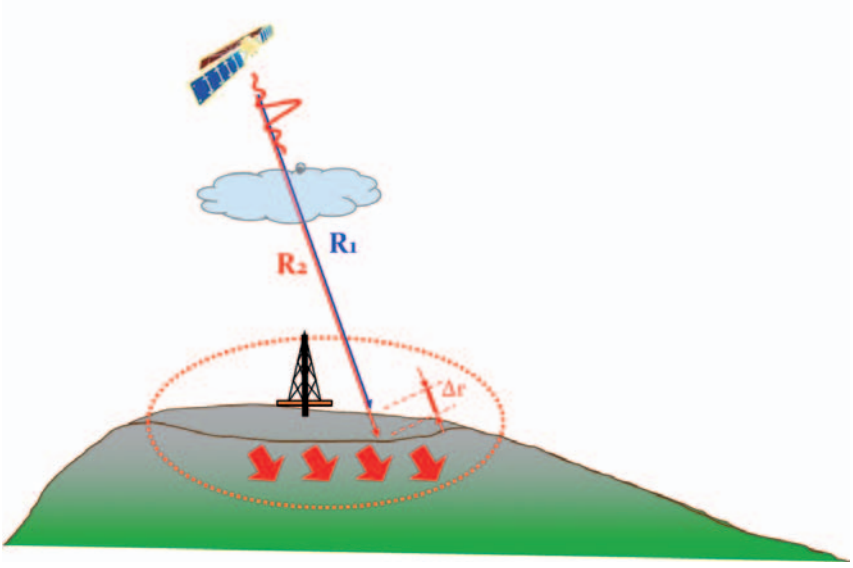

Figure 2 *A schematic showing the relationship between ground displacement and range changes measured through interferometry.*

The squeeSAR approach

To overcome the inaccuracy in the measurements provided by conventional DInSAR, we have developed a multi-image approach, called SqueeSAR, which requires the availability of a long time series of SAR data. The first objective of the algorithm is to identify stable radar targets and then, in correspondence to those targets, estimate and remove the phase term related to atmospheric noise from all the SAR data. Looking for targets with good phase stability we can identify in the data-stack coherent radar targets exhibiting high phase stability over the whole time period of observation. These targets, only slightly affected by temporal and geometrical decorrelation, often correspond to point-wise deterministic scatterers, generally called permanent scatterers (PS). Man-made structures, boulders and outcrops can all generate good PS (Ferretti et al., 2000).

Displacement time-series can be retrieved also for natural targets where no dominant scatterers can be identified within a certain resolution cell, but typically the estimated time-series of deformation is noisier compared to the signal retrieved for a point-wise bright scatterer, if such kind of targets are processed independently. Rather than corresponding to PS, these measurement points often correspond to image pixels belonging to areas of moderate coherence in some interferometric pairs of the available data-set, where many neighbouring pixels share similar reflectivity values, as they belong to the same object. These targets, referred to as distributed scatterers (DS), usually correspond to debris areas, non-cultivated land with short vegetation or desert areas.

Unlike PS, DS are affected by temporal and geometrical decorrelation (Zebker and Villasenor, 1992; Rocca, 2007; Hanssen, 2001) requiring the evaluation of the data covariance matrix to provide a full statistical characterization and to estimate the noise level in each interferogram. As the covariance matrix has to be sampled, we must first identify

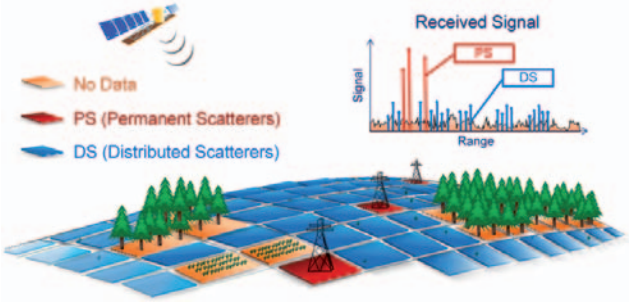

Figure 3 *Image showing the distribution of PS and DS over a typical area of interest with SqueeSAR analysis.*

all the pixels belonging to the same DS, and combine them in a single observation cell. For this purpose, we apply the Kolmogorov-Smirnov test, which is a non-parametric test, in order to identify all the pixels drawn from the same statistical population (Ferretti et al., 2011). Then the sample covariance $\mathbf{\Gamma}$ matrix can be computed for each DS in order to optimally characterize them from a statistical point of view:

$$\mathbf{\Gamma} = \mathrm{E}[\boldsymbol{y}\boldsymbol{y}^{H}] \tag{4}$$

where $\boldsymbol{y}$ is the complex values data vector, $\boldsymbol{y} = [y_1, y_2 \ldots y_N]$ and N is the number of images in the data-set. Absolute values of the off-diagonal elements of $\mathbf{\Gamma}$ are actually an estimate of the noise level (De Zan and Rocca, 2005) for all possible interferograms of the data-stack. The phase values correspond, instead, to spacially filtered interferograms over DS estimated by averaging only pixels which are identified as statistically homogeneous by the Kolmogorov-Smirnov test. For a deterministic radar target, such as a PS, the phase values of all off-diagonal elements of the coherence matrix are redundant: the phase values are simply the difference in phase values of the $N\,(N-1)\,/2N$ (the matrix is hermitian) available SAR scenes, so the following equation holds:

$$\angle\left(\{\Gamma\}_{nj}\right) = \angle\left(\{\Gamma\}_{nm}\{\Gamma\}^{*}_{mj}\right) = \theta_n - \theta_j \quad (5)$$

where the operator $\{\cdot\}_{jm}$ indicates the element of the matrix at row j and column m. In other words, in the case of deterministic radar targets, the property of phase triangularity, or phase consistency, is met by the construction. This is no longer true for a DS. The coherence matrix is not redundant (it is not rank 1) and, in general, equation 5 does not hold.

Indeed, the filtered interferogram generated by image and image is not equal to the phase difference between the filtered interferograms generated using the image pair (n; m) and (m; j); may be just because some of the scatterers belonging to that cell changed their reflectivity in that occasion. Then, for a DS, we are somewhat forced to deal with $N(N-1)/2$ interferometric phase values and not simply N, as with PS. A key problem is then related to the estimation of a vector of N phase values, $\boldsymbol{\theta} = [\theta_1, \theta_2 \ldots \theta_N]$, matching those of the off-diagonal elements of $\boldsymbol{\Gamma}$, properly taking into account the associated coherence values. The adopted solution is to compute a SVD decomposition the coherence matrix:

$$\boldsymbol{\Gamma} = \mathbf{U}\boldsymbol{\Sigma}\boldsymbol{U}^{H} = \sum_{i=1}^{N} \mathbf{U}(:,i)\boldsymbol{\Sigma}(i,i)\boldsymbol{U}^{H}(:,i) \quad (6)$$

If we want to model the matrix as the outer product between one vector and its conjugate, in order to guarantee the phase consistency, its best least square approximation is simply obtained by taking only the first term of the SVD decomposition (Ferretti et al., 2011):

$$\boldsymbol{\Gamma} \approx \mathbf{U}(:,1)\boldsymbol{\Sigma}(1,1)\boldsymbol{U}^{H}(:,1) \quad (7)$$

From a physical point of view, U(: , 1) represents the optimal estimate of the complex reflectivity vector of the DS. Otherwise it can be imagined as a pseudo-PS synthesizing the whole statistical population of the distributed targets. Once we have applied this procedure for all DS, both PS and DS are described by N phase values and therefore can be optimally processed together aimed at retrieving a time-series of displacement for all reliable points.

The advantage of a multi-image approach, such as SqueeSAR, comes from the possibility to identify, through a statistical characterization, good radar targets and to distinguish between displacement and atmospheric effects considering their different statistical behaviours. While surface displacement is correlated in time, the atmospheric noise is uncorrelated in time and correlated in space. It is the ability to remove the two main noise sources of SAR data that makes it possible to reach a high accuracy in the measurements.

At the end of this analysis for each measurement point an accurate elevation, an average displacement rate and a time-series of displacement are provided. The precision of the measure of displacement depends on many parameters such as:

- Spatial density and the quality of reliable measurement points
- Climatic conditions at the time of the acquisitions
- Satellite revisit time
- Total time period spanned by the dataset

In Figure 4 we analyzed the impact of the satellite revisit time, which depends on the specific satellite used for the analysis. We considered the four most currently used satellites for interferometry:

- Envisat, a satellite working in the C-band with a wavelength of about 5.6 cm and a revisiting time of 35 days
- RADARSAT, a satellite working in the C-band with a wavelength of about 5.6 cm and a revisiting time of 24 days

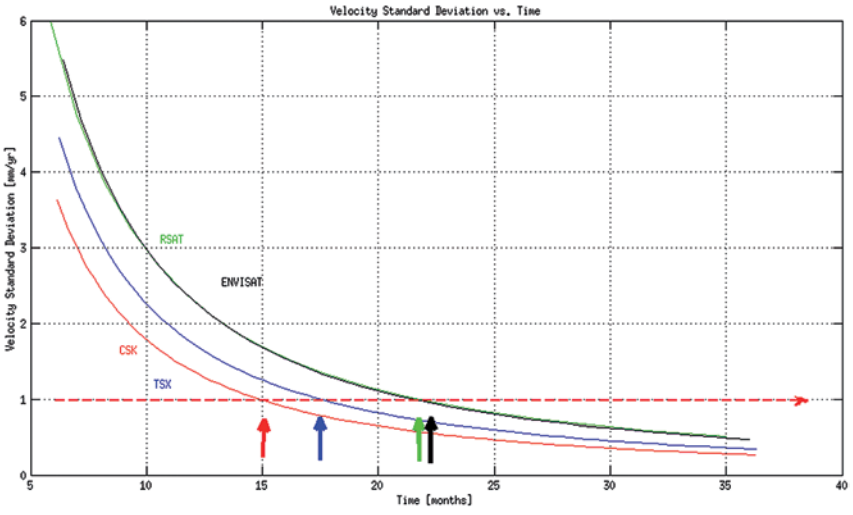

Figure 4 *Standard deviation of the estimated average displacement rates for different satellites as a function of time for an average atmospheric noise mean square delay.*

www.firstbreak.org © 2013 EAGE

- TerraSAR-X, a satellite working in the X-band with a wavelength of about 3.1 cm and a revisiting time of 11 days
- Cosmo-SkyMed, a costellation of four satellites working in the X-band with a wavelength of about 3.1 cm and a revisiting time of eight days

The graph shows that, in order to obtain a millimetric precision, for a TerraSAR-X or Cosmo-SkyMed dataset only 15–18 months of acquisitions are required, corresponding to about 40–50 images. To get the same accuracy with the C-band sensors now available, namely Envisat or RADARSAT, at least two years of acquisitions are required. The curves are computed according to a linear regression model, where the parameter to estimate is the average displacement rate and the noise affecting the data is the atmospheric noise characterized by a certain power σ^2_{APS}. The accuracy σ^2_v of the estimated velocity can be computed, therefore, using the following equation [4]:

$$\sigma_v^2(\Delta t, N, \sigma^2_{APS}) = \frac{\sigma^2_{APS}}{(Bt - \mathrm{E}[Bt])^T (Bt - \mathrm{E}[Bt])} \quad (8)$$

Where σ^2_{APS} is an average atmospheric noise power, inferred from a statistic based on tens of dataset, $Bt = \Delta t\,[0 : N-1]$ is the vector of the temporal baselines of the available N images and Δt is the satellite revisit time. The center frequency, the spatial resolution, the Signal to Noise Ratio, the revisit time all impact on Formula 8, and the outcome of the calculations is shown in Figure 4.

Reservoir monitoring applications

Knowledge of the structure controlling the fluid/gas flow at the reservoir layer is critical in many activities, such as oil/gas extraction and carbon capture and sequestration (CCS). To this end, time-lapse geophysical observations are considered as an important instrument to better understand the fluid flow in the subsurface. In the last decade, multi-image SAR interferometry is receiving increasing attention, thanks to its ability to provide accurate, large-scale surface deformation measurements with millimetric precision. The utility of such data for reservoir monitoring and modelling, has been proven for the first time in the InSalah project, one of the three most famous CCS projects, at the Krechba field. SAR data has been used to track the injected CO_2 (Vasco and Ferretti, 2005), to estimate the effective permeability of a producing gas reservoir and to monitor possible fault reactivation.

Monitoring possible fault reactivation

In the InSalah project large amounts of CO_2 (more than three million tons), instead of being vented into the atmosphere, are injected into a depleted reservoir. The storage of such a large CO_2 volume at depth induces high pressure changes which are expected to lead to the expansion of the reservoir layer.

But, in the case of fractured reservoir, the induced high pressure variations can cause the opening of tensile features at depth, compromising the integrity of the cap-rock and, as a consequence, preventing the CO_2 from remaining within the reservoir. The surface deformation measurements obtained by the analysis of a dataset of SAR images make it possible to identify for the first time such kind of feature due

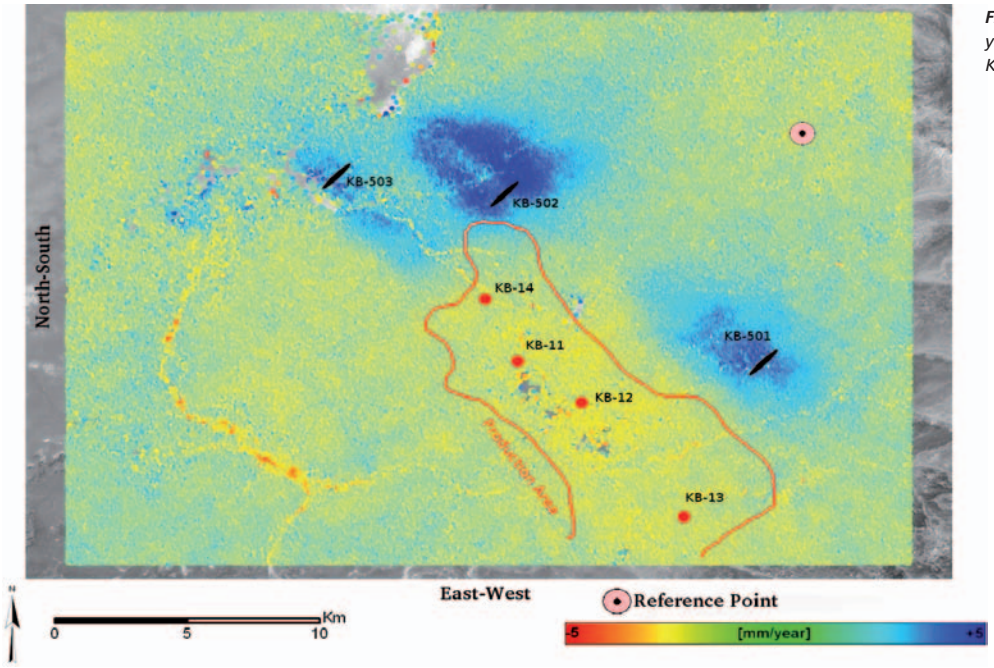

Figure 5 *Average velocity map [mm/yr] measured by SqueeSAR over the Krechba field.*

to CO_2 sequestration. It is possible to determine a map of the average displacement rate shown in Figure 5, this result was obtained processing 41 radar images, covering the period from 2003 through 2008.

In the area under analysis we have three horizontal injection wells (labelled as KB-501, KB-502, and KB-503) located in the northern and eastern areas of the field at the boundaries of the producing reservoir. While the elongated patterns of uplift over KB-501 and KB-503 suggest north–west trending high permeability, features that may reflect fault or fracture zones controlling the flow (Vasco et al., 2008), above the injector KB-502 a double lobed pattern is well visible suggesting the opening of a tensile feature at depth, such as a fault or fracture (Davis, 1983). Based on dislocation theory (Okada, 1985; Steketee, 1958), we can relate surface displacement to fault/fracture dislocation at depth. Estimated parameters are the geometrical configuration of the fault and the amount of dislocation/opening. While the inverse problem is linear with respect to dislocation, it is not linear for the geometrical parameters of the fault, such as the length, width, dip-angle, strike angle, and location. For this reason we first perform a non-linear optimization of the fault parameters considering a constant amount of opening along for the entire fault plane (Rucci et al., 2013). Actually, due to spatial variations in the hydrological properties, the flow and pressure changes at depth may be quite heterogeneous. Furthermore, the geomechanical properties may also vary and the resulting fluid pressure changes can lead to varying amounts of fault/fracture aperture changes. Therefore, we shall allow for spatially-varying fault/fracture aperture changes within designated source regions. We divide the fault plane into smaller size patches for which we want to estimate the magnitude of dislocation $\mathbf{d}$ from the measured surface displacement $\mathbf{u}$:

$$\begin{aligned} \mathbf{u} &= \mathbf{T}\mathbf{d} \\ \mathbf{d} &\geq \mathbf{0} \end{aligned} \tag{9}$$

where $\mathbf{T}$ is the sensitivity matrix corresponding to the tensile dislocations (fault/fracture aperture change) determined by the nature of the medium. Note that, through the last inequality, we require positive dislocation values under the assumption that fluid injection leads only to fault/fracture opening. As the inverse problem is often ill-posed and does not have a unique solution (Parker, 1994), we have to introduce additional constraints:

$$\begin{aligned} \hat{\mathbf{d}} = arg \min_{\mathbf{d}} (&|\mathbf{d} - \mathbf{T}\mathbf{u}|_2 \\ &+ \alpha_d |\mathbf{D}\mathbf{d}|_2 \\ &+ \alpha_r |\mathbf{R}\mathbf{d}|_2) \end{aligned} \tag{10}$$

As indicated in Rucci et al., 2010, 2013], such penalty terms may include a weighted measurement of model norm, model roughness $\mathbf{R}$, and a distance measurement $\mathbf{D}$ penalizing changes far from the injection point. The distance penalty corresponds to the assumption that the largest aperture changes should occur at, or near, the injection point. In Figure 6 we show the distribution of the tensile opening features on the fault/fracture plane, the orientation of the fault plane is north/west–south/east, in agreement with the direction of the regional fault system.

We believe that surface deformation measurement can be used jointly with seismic data to better constrain the geomechanical inversion as the two data-set may provide complementary contributes. It is worth highlighting that the magnitude of the dislocations in Figure 6 is in the order of centimetres, such variation in the structure of the overburden may generate strain distributions hard to identify and measure through seismic. On the contrary, inversion from surface deformation data solely lead to an uncertainty of few hundreds of metres in the vertical location of opening features, an issue which can be overcome in the inversion seismic analysis.

Notice that the total volume of the faulted areas is about 0.6 million cubic metres, of the same order of magnitude of the total injected CO_2.

Permeability estimation

One effect of any significant fluid extraction from a reservoir is that the reservoir, and subsequently the overburden can deform measurably over time. So, deformation in the overburden proves useful in deducing spatial and temporal changes in the volume of a reservoir and, by inference, changes in reservoir pressure. Based upon these changes we can estimate diffusive travel times, and then, as the solution of a linear inverse problem, the effective permeability of the reservoir. An advantage of this approach is that, in comparison to traditional methods based on the inversion of pressure changes amplitude, travel times are less sensitive to the exact geomechanical properties of the reservoir and overburden (Rucci et al., 2013).

As we use a steady-state formulation, the elastic and the fluid/gas pressure field diffusive equations result uncoupled. That implies that changes in fluid pressure field do produce stress and strain, but changes in the stress or strain fields are assumed to not affect fluid pressures. According to this formulation, when the overburden behaves elastically, as described in (Rucci et al. 2010), we may formulate the relationship between the displacement vectors $\mathbf{u}(t)$ and the volume changes at the reservoir layer $\mathbf{v}(t)$, for a certain time t:

$$\mathbf{u}(t) = \mathbf{G}\mathbf{v}(\mathbf{t}) \tag{11}$$

where the columns of matrix $\mathbf{G}$ represent the Green's functions relating volume changes at a certain location to surface deformation and are determined by the nature of the medium in which the reservoir lies. The reservoir layer undergoes a fractional volume change due to changes in fluid pressure. Therefore, once volume changes are computed, they can

www.firstbreak.org © 2013 EAGE

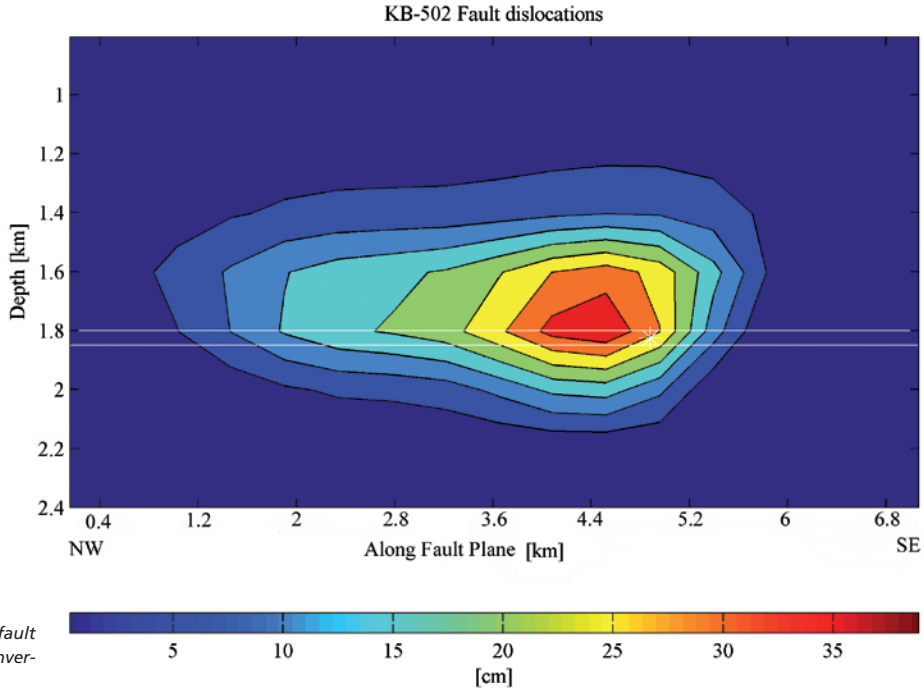

Figure 6 *Aperture change on a sub-vertical fault intersecting well KB- 502, resulting from an inversion of the SAR data.*

be mapped into pressure changes through a simple linear transformation.

Starting from the pressure changes we can infer the permeability solving the diffusive equation governing the evolution of the fluid pressure within the reservoir. For gas the situation is somewhat more complicated due to the compressibility of the gas. That is, the density of a gas is a strong function of the gas pressure (Muskat, 1946; Aronofsky and Jenkins, 1954). Fortunately, there is an integral transformation from the physical pressure $p(x; t)$ to a new variable $\hat{p}(x; t)$, given by Al-Hussainy et al. (1966) which satisfies the diffusion equation:

$$\nabla \cdot (K \nabla P) = C_e \frac{\partial P}{\partial t} \tag{12}$$

where K is the absolute permeability and C_e is the coefficient relating fluid pressure variations to changes in porosity. As shown by Virieux et al. (1994), an asymptotic representation of the solution to the diffusion equation is provided by a series of inverse powers. Substituting the asymptotic series representation into the diffusion equation 12 produces an eikonal equation for the function σ, which is referred to as the phase or pseudo-phase function:

$$\nabla\sigma \cdot \nabla\sigma - k = 0 \tag{13}$$

where $k = C_e / K$ is the relative permeability. In order to avoid the requirement of ray-tracing to solve the eikonal equation 13, we recall the physical interpretation of σ (**x**), pointed out by Virieux et al. (1994), according to which:

$$\sigma = \sqrt{6T_{peak}} \tag{14}$$

where, for a step-function source, T_{peak} is the time at which the time derivative of the pressure change p (x; t) is a maximum [22]. In case of a different kind of source, with a generic temporal evolution, it is necessary first to deconvolve the pressure time-series by the time-series of the injected/extracted cumulative fluid volume. Expressing the eikonal equation in ray coordinates, we can write the phase function as an integral (Vasco et al., 2000, 2008):

$$\sigma(\mathbf{x}) = -\int_{\mathbf{X}(l)} \sqrt{k}\, dl \tag{15}$$

where **X** (l) is the trajectory from the production well to the point in the reservoir at which the volume change is being calculated or estimated.

Then, discretizing equation 15, it can be written a system of linear equations:

$$\mathbf{\Sigma} = \mathbf{L}\,\mathbf{y} \tag{16}$$

where **Σ** is the vector of the phase estimates at the reservoir layer (obtained applying equation 14), **L** is a coefficient matrix which contains the trajectory lengths in each grid block of the reservoir model and **y** is a vector whose components are the average value of $\sqrt{k}$ in each grid block (Vasco et al., 2000). Given equations 16 and 14 the permeability can be estimated solving a simple linear system.

© 2013 EAGE www.firstbreak.org

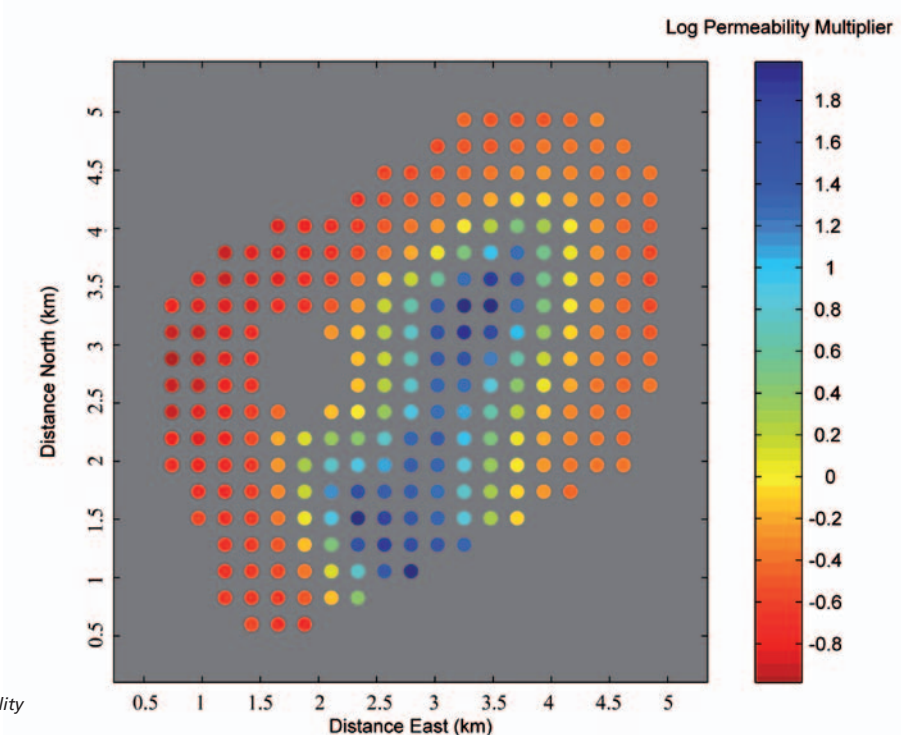

Figure 7 *Logarithm of the relative permeability obtained from an inversion of the travel times.*

The methodology described above has been applied to estimate the relative permeability of a producing gas reservoir located at the Krechba field, in particular we focused on the region surrounding the first pumping well, KB-11. In Figure 7 we show the estimated relative permeability using a logarithmic scale. We can identify two high permeability regions which correlate well with the location of two fault/fractures identified by a previous seismic survey.

Conclusions

This work has highlighted how the availability of precise and spatially dense measurements make it possible to use surface displacement information for reservoir monitoring, modelling, and characterization. Advanced InSAR techniques recently developed are capable, in fact, of achieving millimetre precision, comparable to optical levelling, and a high spatial density of displacement measurements over long periods of time, without the need to install ground-based equipment or otherwise access the study area.

In particular, by applying the SqueeSAR approach, we are able to provide accurate measurements not only for deterministic targets, such as PS, but also for DS, affected by temporal and geometrical decorrelation, leading to an increase in the density of measurement points. This represents a fundamental aspect for improving the modelling and ensuring safer monitoring activities.

Therefore we have shown how SAR data can be used to invert surface deformation information for geophysical parameters at depth, both in the case of gas/oil production and Carbon Dioxide sequestration. In the case of a producing reservoir, we can map surface deformation into pressure changes at the reservoir layer and then infer reservoir permeability. Moreover surface data can be used for the monitoring of CO_2 sequestration induced events. Then, the high pressure variation induced can lead to volume increases confined to the reservoir layer or can induce the reactivation of pre-existing faults. In this case, surface displacements can be mapped to dislocations along the fault plane. The analysis carried out on well KB-502 inferred an amount of opening in the order of centimetres, suggesting that it would have been hard to identify this phenomena through a 4D seismic analysis.

References

Al-Hussainy, R., Ramey, Jr., H. J. and Crawford, P.B. [1966] The flow of real gases through porous media. *Journal of Petroleum Technology*, **18**, 624–636.

Aronofsky J. S., and Jenkins R. [1954] A simplified analysis of unsteady radial gas flow. *Transactions of the American Institute of Mechanical Engineering*, **201**, 149–192.

Curlander, J. and McDonough, R. [1992] *Synthetic Aperture Radar: System and Signal Processing*. Wiley.

Davis, P.M. [1983] Surface deformation associated with a dipping hydrofracture. *J. Geophy. Res*, **88**, 5826–5834.

De Zan, F. and Rocca, F. [2005] Coherent processing of long series of SAR images, *Proceedings IGARSS*, Seoul, 1987–1990.

Ferretti, A., Fumagalli, A., Novali, F., Prati, C., Rocca, F. and Rucci A. [2011] A new algorithm for processing interferometric data-stacks: SqueeSAR.

IEEE Trans. on Geoscience and Remote Sensing, doi: 10.1109/TGRS.2011.2124465.

Ferretti, A., Monti Guarnieri, A., Prati, C. and Rocca F. [2007] *InSAR principles: Guidelines for SAR Interferometry Processing and Interpretation* (Ed. Fletcher, K.), www.esa.int/esapub/tm/tm19/TM-19 ptA.pdf; www.esa.int/esapub/tm/tm19/TM-19ptB.pdf; www.esa.int/esapub/tm/tm19/TM-19 ptC.pdf.

Ferretti, A., Prati, C. and Rocca, F. [2000] Permanent Scatterers in SAR Interferometry. *IEEE Trans. on Geoscience and Remote Sensing*, **38**(5), 2202–2212.

Hanssen, R. [2001] *Radar Interferometry: Data Interpretation and Error Analysis. Dordrecht, The Netherlands*. Kluwer.

Monti Guarnieri, A., Prati, C. and Rocca, F. [1990] Seismic migration for SAR focusing: interferometric applications. *IEEE Trans. on Geoscience and Remote Sensing*, **28**(4), 627–640.

Muskat, M. [1946] *Flow of Homogeneous Fluids Through Porous Media*. J. W. Edwards, Ann Arbor.

Okada, Y. [1985] Surface deformation to shear and tensile faults in a half-space. *Bull. Seism. Soc. Am.*, **75**, 1135–1154.

Parker, R. L. [1994] *Geophysical Inverse Theory*, Princeton University Press, Princeton.

Rocca, F. [2007] Modeling Interferogram Stacks. *IEEE Trans. on Geoscience and Remote Sensing*, **45**(10), 3289–3299.

Rucci A., Vasco, D.W., and Novali, F. [2010] Fluid pressure arrival-time tomography: Estimation and assessment in the presence of inequality constraints with an application to production at the Krechba field, Algeria. *Geophysics*, **75**, O39–O55.

Rucci, A., Vasco, D.W. and Novali, F. [2013] Monitoring the geologic storage of carbon dioxide using multi-component SAR interferometry. *Geophysical Journal International*, doi: 10.1093/gji/ggs112.

Steketee,J.A. [1958] On Volterra's dislocation in a semi-infinite elastic medium. *Can. J. Phys.*, **36**, 192–205.

Vasco, D.W. and Ferretti, A. [2005] On the use of quasi-static deformation to understand reservoir fluid flow. *Geophysics*, **70**, O13–O27.

Vasco, D.W., Ferretti, A. and Novali, F. [2008] Estimating permeability from quasi- static deformation: Temporal variations and arrival-time inversion. *Geophysics*, **73**, O37–O52.

Vasco, D.W., Karasaki, K. and Keers, H. [2000] Estimation of reservoir properties using transient pressure data: An asymptotic approach. *Water Resources Research*, **36**, 3447–3465.

Virieux, J., Flores-Luna, C. and Gibert, D. [1994] Asymptotic theory for diffusive electro-magnetic imaging. *Geophysical Journal International*, **119**, 857–868.

Zebker, H.A. and Villasenor, J. [1992] Decorrelation in interferometric radar echoes. *IEEE Trans. on Geoscience and Remote Sensing*, **30**(5), 950–959.

EAGE

EUROPEAN ASSOCIATION OF GEOSCIENTISTS & ENGINEERS

EAGE/AAPG Workshop 2013

Basin-Margin Wedge Exploration Plays

20-22 November 2013 - Lisbon, Portugal

In recent decades, the exploration of continental margins has proven successful around the world principally by drilling closures either in extensional provinces (rift or deltaic gliding systems) or in compressive basins (wrench margins or thrust fronts of deltas). In recent years, several significant discoveries have been made in the South Atlantic margins in a new so called "Basin-Margin Wedge Play" which is not controlled by local structural closures but by large scale stratigraphic traps.

The aim of the workshop is to promote discussions on the strengths and failings of such a concept and about the risks associated with each component of the petroleum system: charge, reservoir occurrence and quality, vertical and lateral seals and traps.

Topics:
1. Exploration trends and case-studies
2. Geodynamic and petroleum contexts
3. Associated traps
4. Reservoir challenges

www.eage.org

Call for Papers deadline: 15 July 2013